INTERNATIONAL JOURNAL FOR NUMERICAL METHODS IN FLUIDS, VOL. 7, 567–579 (1987)

A SELF-ADAPTIVE GRIDDING FOR INVISCID TRANSONIC PROJECTILE AERODYNAMICS COMPUTATION

CHEN-CHI HSU

Department of Engineering Sciences, University of Florida, Gainesville, Florida 32611, U.S.A.

AND

CHYUAN-GEN TU

Bureau of Planning, Republic of China Naval Headquarters

SUMMARY

An adaptive grid generation technique based on modified variational principles coupled with an exponential clustering has been developed and tested successfully for the computation of steady inviscid transonic projectile aerodynamics. The isoperimetric problem for adaptive gridding is to extremize a grid smoothness functional subject to grid orthogonality and resolution functionals; however, the Lagrange multipliers have been assumed to be variables with zero variation and are properly chosen as functions of local grid size to enhance locally the grid resolution as well as to maintain the weight of three grid characteristics the same over the entire flow field. With computed pressure gradient as the control function for grid adaptation, the resulting Euler equations cannot provide sufficient grid resolution in the boundary layer region of the projectile geometry; hence, a clustering technique is needed to redistribute the points along the normal grid lines. A grid generation code has been developed and coupled to an axisymmetric thin-layer Navier–Stokes code for self-adaptive grid generation. For the three transonic flow cases considered, $M_\infty = 0{\cdot}91$, $0{\cdot}96$ and $1{\cdot}10$, the distribution of surface pressure calculated from the inviscid option of the Navier–Stokes code is indeed in excellent agreement with published measured data.

KEY WORDS Adaptive Grid Variational Method Transonic Projectile Aerodynamics

INTRODUCTION

An accurate prediction of the aerodynamic drag force is essential to a better design of aerodynamic devices and flight vehicles. Recently a thin-layer Navier-Stokes code has been developed for high speed compressible fluid flow problems.[1] This code can provide acceptably accurate solutions for unsteady or steady inviscid and viscous flow problems if a good grid system is provided; for the viscous case, one can further specify either a laminar flow or a turbulent flow. The turbulence closure model programmed in the code is a two-layer algebraic eddy viscosity model.[2] The Navier–Stokes code has also been simplified for axisymmetric flows to improve the computational effectiveness.[3]

The application of the thin-layer Navier–Stokes code to transonic projectile aerodynamic problems has been investigated by the U.S. Army Ballistic Research Laboratory. The grid network used in the computation is an axisymmetric grid system formed by a sequence of planar

0271–2091/87/060567–13$06.50

Received 10 March 1986
Revised 21 July 1986

grids around the axis of a projectile. The planar grid is obtained from a grid generation code named GRIDGEN.[4] This code can provide either an elliptic or a hyperbolic grid, which is then modified with an exponential clustering along the grid lines normal to the streamwise direction to give sufficient grid resolution for the viscous region. Hence, a good adaptive grid can be obtained for transonic flows past a projectile with sting at zero angle of attack if the boundary grid points are properly chosen. For a secant–ogive–cylinder–boat-tail (SOCBT) projectile with sting (i.e. no base flow) at zero angle of attack and Mach number $M_\infty = 0{\cdot}91$, 0·94, 0·96, 0·98 and 1·10, the computed surface pressure coefficient C_p over the secant–ogive portion and the boat-tail portion of the projectile agrees rather well with the measured data; however, the agreement on the cylinder portion between the shocks, which may be acceptable, is not very satisfactory for some cases considered.[5,6] As reported in Reference 7 a good adaptive planar grid for accurate solutions can be obtained from GRIDGEN only after considerable experimentation with boundary grid positioning. For the projectile model at 2° angle of attack and $M_\infty = 0{\cdot}91$ the C_p distribution computed on a CRAY 1S computer agrees qualitatively with the measured data, but quantitatively the agreement over the cylinder and boat-tail portions is not satisfactory at all.[7] It is believed that the main cause for the unsatisfactory results can be taken to be the use of a grid system which is not properly adaptive to the solution.

A good grid system for fluid dynamics computations can be justified from the smoothness of grids, the orthogonality of grids and the grid resolution adaptive to the solution in the physical space. It had been reported that rapid changes of the grid size and highly skewed grids can result in undesirable errors.[8] It is also well known in approximation that the choice of high grid resolution in regions where the solution gradient is very large is essential to the accuracy of the numerical result. In fact an improper grid resolution in high gradient regions can be detrimental to the solution accuracy as well as to the convergence process of a solution algorithm. There have been a number of adaptive grid generation methods proposed and reported in symposia, workshops, and conferences. The method based on a constrained variational principle, proposed by Brackbill[9] at a symposium, is rather general and seems to be a very promising approach for complex fluid flow problems in which shock waves, flame fronts and viscous layers may cause extremely thin high-gradient regions of unknown location and orientation, since the governing differential equations for an adaptive grid system are derived from minimizing a general variational functional which consists of functionals for measuring the smoothness of grids, the orthogonality of grids and the grid resolution adaptive to a chosen control function. In fact, Saltzman has investigated an application of the adaptive grid generation technique to a two-dimensional inviscid supersonic flow past a step in a wind tunnel.[10] In his study, the adaptive gridding in the domain was controlled by the computed pressure gradient whereas the boundary grids were determine by extrapolation from internal grids out normally to the straight boundary. The unsteady solutions computed for the formation and propagation of shock waves were striking; they showed that the adaptive mesh generator moves the computational grid with shock fronts and consequently enhances significantly the desirable resolution of the finite-difference scheme for the accuracy.

The objective of this study is to explore further the application of variational principles for generating a good adaptive grid to the computation of transonic projectile aerodynamics. Numerical experiments have been carried out to assess the implication and difficulty of the grid generation method and, consequently, an adaptive grid generation technique mainly based on constrained variational principles has been developed and coupled to a thin-layer Navier–Stokes code for SOCBT projectile aerodynamics computations.

VARIATIONAL PRINCIPLES FOR GRID GENERATION

With a boundary conforming transformation an irregular two-dimensional domain Ω in the physical space, xy-plane, can be mapped into a rectangular domain Ω' in the computational space, $\xi\eta$-plane; consequently, a square grid network in the computational space can be constructed for solving boundary value problems. The ξ and η co-ordinates then become the curvilinear coordinates for Ω in the physical space and constant ξ-lines and η-lines form a grid system in Ω. It is known that the co-ordinate transformation yields the metrics

$$\xi_x = \frac{y_\eta}{J}, \quad \xi_y = -\frac{x_\eta}{J}, \quad \eta_x = -\frac{y_\xi}{J}, \quad \eta_y = \frac{x_\xi}{J}, \tag{1}$$

in which J is the Jacobian of the transformation, given by

$$J = x_\xi y_\eta - x_\eta y_\xi. \tag{2}$$

It one chooses $\Delta\xi = \Delta\eta = 1{\cdot}0$ in the computational space, then the Jacobian J represents the grid size in the physical space.

The smoothness of a grid network in the physical space can be measured by the integral

$$I_s = \int_\Omega [(\nabla\xi)^2 + (\nabla\eta)^2]\,dx\,dy. \tag{3}$$

An extremization of this integral with prescribed boundary conditions will result in the Laplace equation; hence, a unique solution exists for the grid. Moreover, the orthogonality of grids can be measured by the integral[11]

$$I_0 = \int_\Omega (\nabla\xi\cdot\nabla\eta)^2 J^3\,dx\,dy, \tag{4}$$

and the grid resolution adaptive to a control function $w(x, y)$ can be represented by

$$I_v = \int_\Omega wJ\,dx\,dy. \tag{5}$$

We note that the term J^3 in equation (4) emphasizes the orthogonality for large grids, and the choice of the cubic power is for the simplification of the resulting governing equations. Therefore, a good grid in the physical space can be measured by the smoothness functional subject to the subsidiary conditions, the orthogonality functional and the grid resolution functional; consequently, an isoperimetric problem for the grid generation is to minimize the functional

$$I = I_s + \bar{\lambda}_0 I_0 + \bar{\lambda}_v I_v, \tag{6}$$

in which $\bar{\lambda}_0$ and $\bar{\lambda}_v$ are Lagrange multipliers.[12]

The introduction of undetermined Lagrange multipliers requires prescribed values for the subsidiary conditions, equations (4) and (5). Since a proper choice of these values for a good grid system is very difficult to make, if not impossible, it is more effective in practice to select values for the Lagrange multipliers. Let L_p and L_c be the characteristic lengths in the physical domain and the computational $\xi\eta$-plane, respectively. Also, denote by W a reference value for the control function $w(x, y)$ in equation (5). We then observe that the integrands of the functionals I_s, I_0 and I_v have the dimensions of $(L_c/L_p)^2$, $(L_p/L_c)^2$ and $W(L_p/L_c)^2$, respectively. Therefore, if the Lagrange multipliers are defined as

$$\bar{\lambda}_0 = \frac{\lambda_0}{\tilde{\lambda}_0} \equiv \lambda_0 \left(\frac{L_c}{L_p}\right)^4, \quad \bar{\lambda}_v = \frac{\lambda_v}{\tilde{\lambda}_v} \equiv \lambda_v \frac{1}{W}\left(\frac{L_c}{L_p}\right)^4, \tag{7}$$

then each term on the right hand side of equation (6) has the same order of magnitude, provided that λ_0 and λ_v are of $O(1)$. The relative importances of the three functionals for grid generation can be identified from the values chosen for λ_0 and λ_v.

For adaptive boundary gridding, a one-dimensional variational principle can be employed. The functional consisting of a smoothness functional and a grid resolution functional can be written as

$$I_B = I_{Bs} + \bar{\lambda}_{Bv} I_{Bv} \equiv \int_B \xi_s^2 \, ds + \bar{\lambda}_{Bv} \int_B w_B(s) s_\xi \, ds. \tag{8}$$

Similarly, the Lagrange multiplier is defined as

$$\bar{\lambda}_{Bv} = \frac{\lambda_{Bv}}{\tilde{\lambda}_{Bv}} \equiv \lambda_{Bv} \frac{1}{W_B}\left(\frac{L_{BC}}{L_{BP}}\right)^3, \tag{9}$$

where L_{BP}, L_{BC} and W_B are characteristic quantities.

GOVERNING EQUATIONS FOR GRID GENERATION

If a physical problem is to be solved in the transformed rectangular domain, the matrics of transformation must be provided. This implies that a curvilinear grid in the physical domain must be generated; consequently, the dependent variables and the independent variables of the functionals have to be interchanged. Accordingly, applying the relation $dx\,dy = J\,d\xi\,d\eta$ and the metric relations, equation (1), the general functional for grid generation, equation (6), becomes

$$I = \int_{\Omega'} \frac{1}{J}[x_\xi^2 + x_\eta^2 + y_\xi^2 + y_\eta^2]\,d\xi\,d\eta + \bar{\lambda}_0 \int_{\Omega'} [x_\xi x_\eta + y_\xi y_\eta]\,d\xi\,d\eta$$
$$+ \bar{\lambda}_v \int_{\Omega'} w(x,y) J^2 \,d\xi\,d\eta, \tag{10}$$

in which the Jacobian J is defined in equation (2). Hence the governing equations for grid generation are the Euler equations resulting from extremizing the functional I, provided that $x(\xi,\eta)$ and $y(\xi,\eta)$ are prescribed on the boundary. They are the following two quasilinear elliptic differential equations:

$$\begin{aligned} a_1 x_{\xi\xi} + a_2 x_{\xi\eta} + a_3 x_{\eta\eta} + b_1 y_{\xi\xi} + b_2 y_{\xi\eta} + b_3 y_{\eta\eta} + \tfrac{1}{2}\bar{\lambda}_v w_x J^2 = 0, \\ b_1 x_{\xi\xi} + b_2 x_{\xi\eta} + b_3 x_{\eta\eta} + c_1 y_{\xi\xi} + c_2 y_{\xi\eta} + c_3 y_{\eta\eta} + \tfrac{1}{2}\bar{\lambda}_v w_y J^2 = 0. \end{aligned} \tag{11}$$

Here the coefficients a_i, b_i and c_i for $i = 1, 2$ and 3 are given by

$$\begin{aligned} a_i &= a_{si} + \bar{\lambda}_0 a_{0i} + \bar{\lambda}_v w(x,y) a_{vi}, \\ b_i &= b_{si} + \bar{\lambda}_0 b_{0i} + \bar{\lambda}_v w(x,y) b_{vi}, \\ c_i &= c_{si} + \bar{\lambda}_0 c_{0i} + \lambda_v w(x,y) c_{vi}, \end{aligned}$$

in which

$$\begin{aligned} a_{s1} &= \alpha A, & a_{s2} &= -2\beta A, & a_{s3} &= \gamma A, \\ b_{s1} &= -\alpha B, & b_{s2} &= 2\beta B, & b_{s3} &= -\gamma B, \\ c_{s1} &= \alpha C, & c_{s2} &= -2\beta C, & c_{s3} &= \gamma C, \end{aligned}$$

$$A = y_\xi^2 + y_\eta^2, \qquad B = x_\xi y_\xi + x_\eta y_\eta, \qquad C = x_\xi^2 + x_\eta^2,$$

$$\alpha = \frac{1}{J^3}(x_\eta^2 + y_\eta^2), \qquad \beta = \frac{1}{J^3}(x_\xi x_\eta + y_\xi y_\eta), \qquad \gamma = \frac{1}{J^3}(x_\xi^2 + y_\xi^2),$$

$$a_{01} = x_\eta^2, \qquad a_{02} = 2(2x_\xi x_\eta + y_\xi y_\eta), \qquad a_{03} = x_\xi^2,$$

$$b_{01} = x_\eta y_\eta, \qquad b_{02} = x_\xi y_\eta + x_\eta y_\xi, \qquad b_{03} = x_\xi y_\xi,$$

$$c_{01} = y_\eta^2, \qquad c_{02} = 2(x_\xi x_\eta + 2y_\xi y_\eta), \qquad c_{02} = y_\xi^2,$$

$$a_{v1} = y_\eta^2, \qquad a_v = -2y_\xi y_\eta, \qquad a_{v3} = y_\xi^2,$$

$$b_{v1} = -x_\eta y_\eta, \qquad b_{v2} = x_\xi y_\eta + x_\eta y_\xi, \qquad b_{v3} = -x_\xi y_\xi,$$

$$c_{v1} = x_\eta^2, \qquad c_{v2} = -2x_\xi x_\eta, \qquad c_{v3} = x_\xi^2.$$

Similarly the governing differential equation for adaptive boundary gridding can be derived from equation (8). One finds

$$[1 + \bar{\lambda}_{Bv} w_B(s) s_\xi^3] s_{\xi\xi} + \tfrac{1}{2}\bar{\lambda}_{Bv} \frac{dw_B}{ds} s_\xi^5 = 0, \tag{12}$$

in which s is the distance measured along the boundary. It is mentioned in passing that an improper choice of $\bar{\lambda}_0, \bar{\lambda}_v$ and $w(x, y)$ in equation (10) can change the type of differential equations (11).

NUMERICAL EXPERIMENTS AND RESULTS

Transonic inviscid flows past a SOCBT projectile with sting at zero angle of attack have been considered for the study. This projectile model has a 3-caliber secant-ogive part followed by a 2-caliber cylinder and 1-caliber 7-degree boat-tail which is further extended for another 1·77 calibers to meet a horizontal sting. There are surface pressure measurements available for assessing the accuracy of numerical results.[6] The physical domain of the problem considered contains about 4 projectile-lengths from the nose, 5 projectile-lengths from the cylinder and 3 projectile-lengths downstream of the base. The transonic aerodynamics problem is solved by an axisymmetric thin-layer Navier–Stokes code obtained from the U.S. Army Ballistic Research Laboratory. In this code the transformed thin-layer Navier–Stokes equations are solved by the Beam and Warming scheme in which a second-order implicit dissipation term and a fourth-order explicit dissipation term have been added for controlling the numerical stability. The code has an option for solving inviscid flow problems and a steady solution results from a converged solution of the unsteady problem. It is mentioned in passing that a planar grid must be generated and provided to the code for the aerodynamics computation.

All planar grids generated and used in this study consist of 70 × 35 grid points with 70 points along the surface of the projectile model; hence, the range of (ξ, η) in the computational space is from (1, 1) to (70, 35). Moreover, resulting from experience with the limited numbers of points used, we have fixed the distribution of the number of boundary points along the projectile model as follows: 23 points on the ogive, 22 points on the cylinder, 17 points on the boat-tail and 8 points on the sting. For grid generation, the governing partial differential equations (11), are approximated by second-order central difference schemes and the resulting non-linear algebraic equations are solved by the Newton–Raphson interactive method supplemented with overrelaxation. The boundary conditions for $x(\xi, \eta)$ and $y(\xi, \eta)$ at the projectile surface $\eta = 1$ and at the outer boundary $\eta = 35$ are predetermined by equation (12) for grid resolution; however, the conditions at the side boundaries, $\xi = 1$ and $\xi = 70$, are obtained and updated by extrapolation from inner grids at the

end of each iteration. We note that the extrapolation technique for determining boundary grids on the projectile surface can be detrimental because of the complex geometry.

The generation of a good adaptive grid based on the variational principle depends on a proper choice of the control function $w(x, y)$ in equation (5) for grid resolution as well as suitable choices of the Lagrange multipliers $\bar{\lambda}_0$ and $\bar{\lambda}_v$ defined in equation (7), provided that good adaptive boundary grids are prescribed. For the transonic flow problems considered, the variation of solutions in the domain of interest is dominated by the pressure field and, therefore, we have chosen the control function for grid adaptation as

$$w(x, y) = |P_x| + |P_y|, \tag{13}$$

in which P_x and P_y are components of the computed pressure gradient. A converged solution of the projectile problem at a Mach number of 0·96 has been used to investigate the relative importance of the multipliers on the grid resolution functional I_v; with $\bar{\lambda}_0 = 1$ and $\bar{\lambda}_v$ varying from 0 to 10, the variance of I_v over the mean of I_0 changes from 9·0 to 7·8. This implies that different choices of the multipliers will have rather minimal effects on grid resolution adaptive to the control function. Hence, we have assumed for the following study that

$$\lambda_0 = \lambda_v = \lambda. \tag{14}$$

Note that λ_0 and λ_v are related to the corresponding multipliers by equation (7). The choice of $\lambda = 1$ implies that the grid generated has the same weight on the three grid characteristics, whereas the grid orthogonality and grid resolution can be enhanced over the smoothness by increasing the value of λ.

For assessing the application of the adaptive grid generation technique, we have considered the projectile aerodynamics problem at $M_\infty = 0{\cdot}91$. The characteristic lengths L_p and L_c in equation (7) are the global ones similar to those used by Saltzman, and λ is set to 4·0. The initial grid provided to the thin-layer Navier–Stokes code is a smooth one. The computed surface pressure coefficient C_p after 50 time steps, i.e. NT = 50, is shown in Figure 1(a); measured data

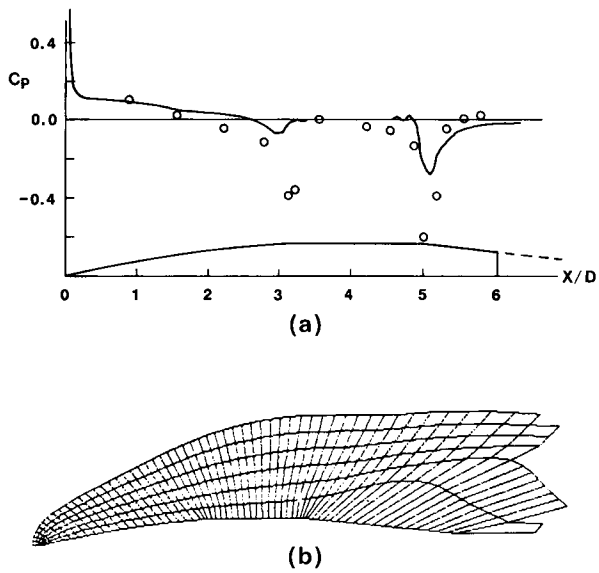

Figure 1. Surface pressure coefficient computed and adaptive grid generated at NT = 50 for $M_\infty = 0{\cdot}91$. (a) ——: computed transient C_p; ○: measured steady state C_p. (b) Grid generated near the projectile model surface

for the steady solution are also plotted for reference. A new grid adaptive to the computed pressure gradient at NT = 50 is then generated for continuation of the solution code. Figure 1(b) shows the grid network near the projectile. The thin-layer code is restarted for another 150 steps, i.e. NT = 200, and the computed pressure coefficient is shown in Figure 2(a). Apparently, the solution is not converging correctly, which can be attributed to the poor grid used in the computation. A new grid adaptive to the computed pressure gradient at NT = 200 is again generated for the restart of the solution process. As shown in Figure 3, the result obtained at NT = 350 does not seem to be properly converging either, even though the grid used looks

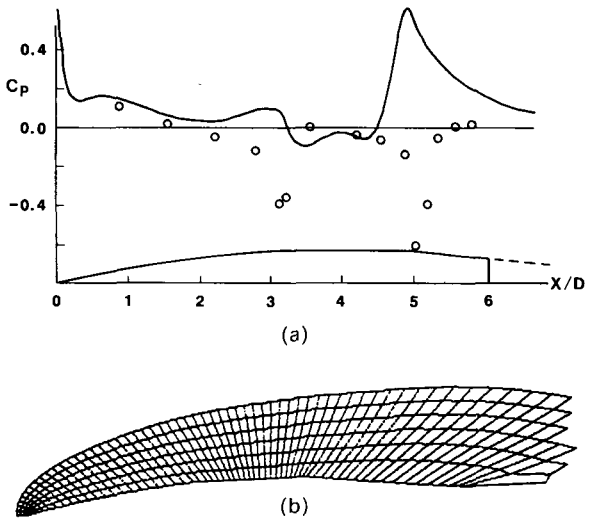

Figure 2. Surface pressure coefficient computed and adaptive grid generated at NT = 200 for $M_\infty = 0{\cdot}91$. (a)——: computed transient C_p; ○: measured steady state C_p. (b) Grid generated near the projectile model surface

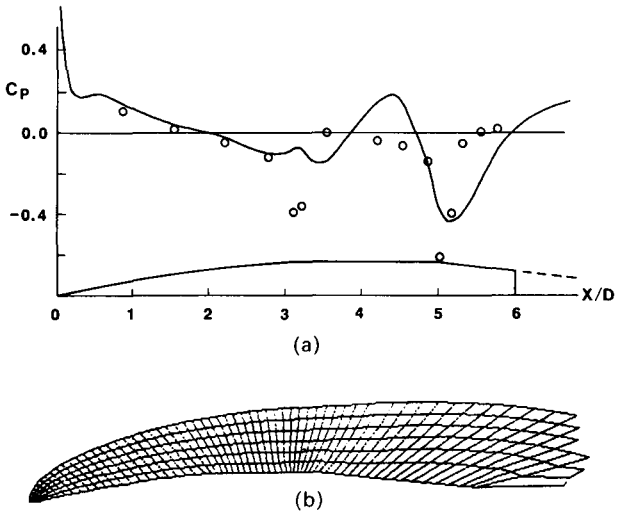

Figure 3. Surface pressure coefficient computed and adaptive grid generated at NT = 350 for $M_\infty = 0{\cdot}91$. (a)——: computed transient C_p; ○: measured steady state C_p. (b) Grid generated near the projectile model surface

better than the one used previously; moreover, we note that the updated adaptive grid at NT = 350 is very similar to that at NT = 200. The continuation of the solution algorithm with the updated grid has failed within the next 150 steps.

A close examination of the planar grids generated clearly indicates that the grid characteristics right next to the projectile are rather poor; in particular, the grid resolution is not sufficient. This implies that the effect of boundary geometry on a good grid generation has to be investigated and considered in the control function. In this study, however, the difficulty is overcome by applying an exponential clustering[4] along η-lines of the adaptive grid generated with the smallest spacing equal to 0·01 at the projectile. An adaptive grid with clustering generated at NT = 350 is shown in Figure 4(a). With this new grid the thin-layer code provides a converging solution at NT = 500, as evidenced from the result shown in Figure 4(b). The process has been repeated and the distribution of C_p computed at NT = 650 indeed shows better agreement with the measured data.

The adaptive gridding with exponential clustering is next tested on the projectile problem at $M_\infty = 0{\cdot}96$. The first adaptive grid is again generated at NT = 50, but subsequent new grids are generated after every 200 time steps. The solution process proceeded smoothly without any difficulty and provided an acceptably accurate pressure distribution at NT = 850. For assessing the grid generation technique, however, the integration process was carried out further to NT = 1650. Figure 5 shows the agreement between the computed C_p at NT = 1650 and measured data; however, appreciable differences observed on the cylinder and its junction with the boat-tail still call for better grid resolutions in those regions.

The choice of the control function $w(x, y)$ to obtain a better adaptive grid is not a trivial one; it requires extensive parametric study and numerical experimentation. For instance, we have used a stronger control function equal to the square of the pressure gradient and experienced overflow

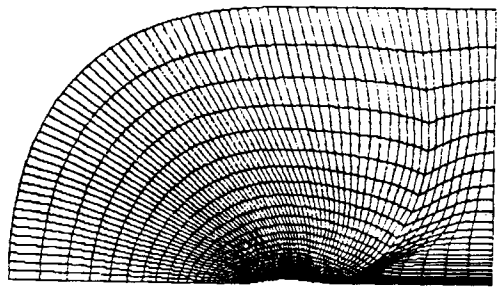

(a)

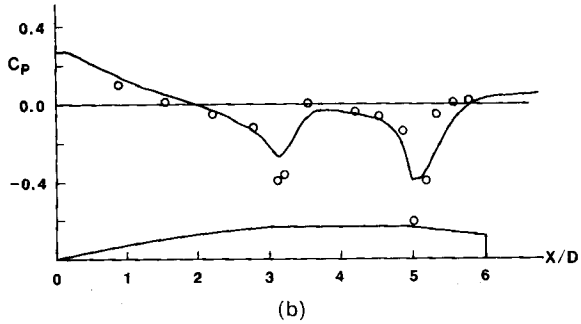

(b)

Figure 4. Adaptive grid with clustering and computed surface pressure coefficient for $M_\infty = 0{\cdot}91$: (a) adaptive grid with clustering generated at NT = 350; (b) C_p distribution computed at NT = 500

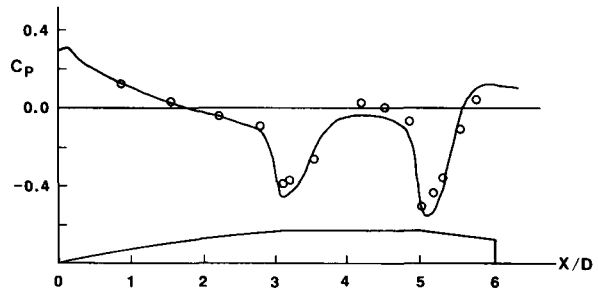

Figure 5. Converged C_p distribution computed at NT = 1650 with self-adaptive gridding for $M_\infty = 0{\cdot}96$.

in the process of grid generation. However, the expression for the general functional, equation (6), shows that the grid resolution can be enhanced by choosing a larger value for the multiplier $\bar{\lambda}_v$, that is a large λ_v defined in equation (7). Unfortunately, the use of an extremely large λ_v can be detrimental to the grid generation also. Moreover, a good adaptive grid should have not only good adaptive grid resolutions but also good orthogonality and smoothness characteristics. Therefore, the parameter $\lambda_v = \lambda_0 \equiv \lambda$ has to be of the order of magnitude one, or ten at most. For the projectile problem considered, the use of a large λ and global characteristic lengths for the multipliers has not resulted in a better adaptive grid. We observe that the grid resolution functional I_v of equation (5) can be considered as a limiting case of the general functional; consequently, the variational principle of I_v will give a grid best adaptive to the chosen control function $w(x, y)$. Apparently, the control function used in this study, equation (13) does not provide sufficient grid resolutions for the transonic flow problems.

The variational principle of the general functional I, equation (6), indicates that the effect of the grid resolution functional can be enhanced locally if a variable Lagrange multiplier $\bar{\lambda}_v$ is used. Departing from the classical variational principle by assuming the variation of the Lagrange multipliers $\bar{\lambda}_0$ and $\bar{\lambda}_v$ to be zero, the variation of I equal to zero will result in exactly the same Euler equations (11), for grid generation. Now the variable $\bar{\lambda}_0$ and $\bar{\lambda}_v$ defined in equation (7) must be selected. In order to realize the relative weight of each term in equation (6) we have fixed the parameters λ_0 and λ_v and assumed the relation (14) in grid generation; accordingly, the reference quantities L_c, L_p and W are considered to be variables. In the following study we have chosen the local grid spacings as well as local values of the control function for the referenced quantities; hence, L_c of the computational space is equal to one. Equation (7) indicates that grid resolutions will be further enhanced locally in the region of small grids (i.e. small L_p), even though the weight of the grid resolution term in equation (6) remains the same. In the process of grid generation, the non-linear governing equations (11), are solved by an iterative method; hence, the local reference length L_p is updated at the end of each iteration. Similarly, equation (12) for adaptive boundary gridding is solved with L_{BP} and W_B defined in equation (9), taken as the local quantities.

The adaptive grid generation technique based on the modified variational principles and a clustering strategy is first investigated on the projectile problem at $M_\infty = 1{\cdot}10$. An adaptive grid generation code has been developed and coupled to the thin-layer Navier–Stokes code with a strategy of adaptive gridding fixed as follows: the first adaptive grid is generated at NT = 50 with $\lambda = 0{\cdot}5$ and subsequently a new grid is generated and used at 150 time steps interval with $\lambda = 1{\cdot}0, 5{\cdot}0, 7{\cdot}5$ and $10{\cdot}0$ at NT = 650 for enhancing the weight of the grid resolution term as the pressure field is being developed. Figures 6–9 show the sequence of results computed to NT = 500. We observe that the solution algorithm is converging very smoothly and highly accurate results have been obtained at NT = 500; moreover, the adaptive grids generated exhibit clearly the

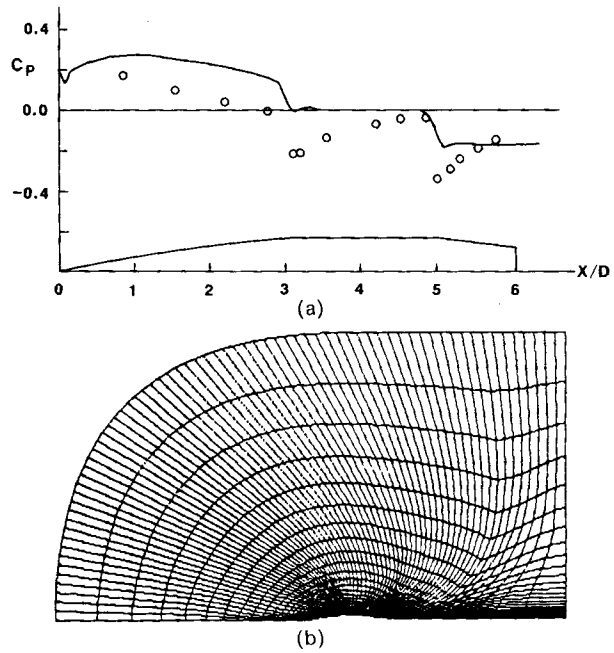

Figure 6. Surface pressure coefficient and adaptive grid at NT = 50 for $M_\infty = 1{\cdot}10$. (a) ——: computed transient C_p; ○: measured steady state C_p. (b) Adaptive grid based on variable $\bar{\lambda}_0$ and $\bar{v}_v$; $\lambda = 0{\cdot}5$

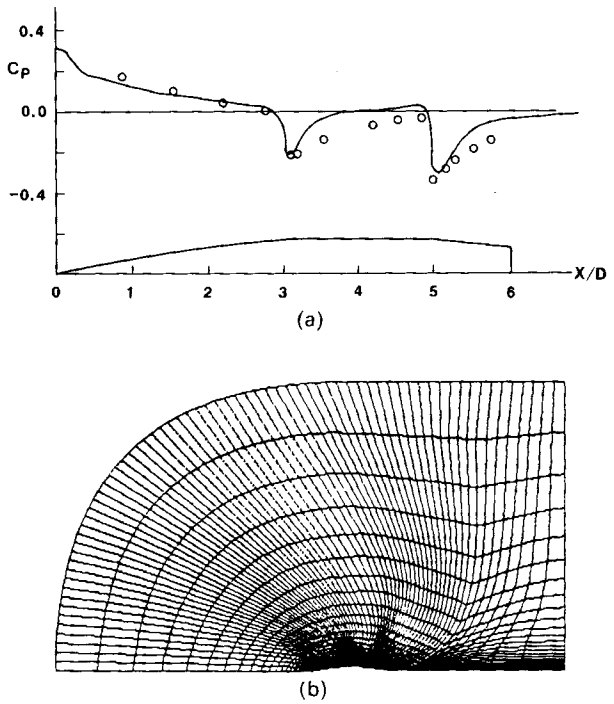

Figure 7. Surface pressure coefficient and adaptive grid at NT = 200 for $M_\infty = 1{\cdot}10$. (a) ——: Computed transient C_p; ○: measured steady state C_p. (b) Adaptive grid based on variable $\bar{\lambda}_0$ and $\bar{v}_v$; $\lambda = 1{\cdot}0$

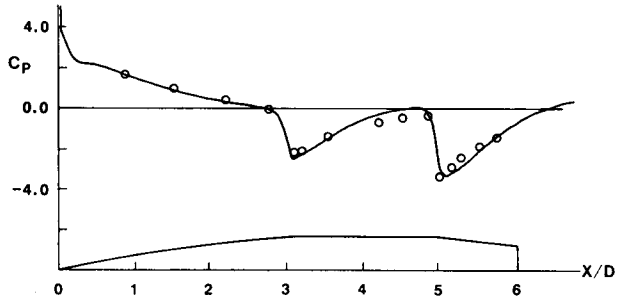

(a)

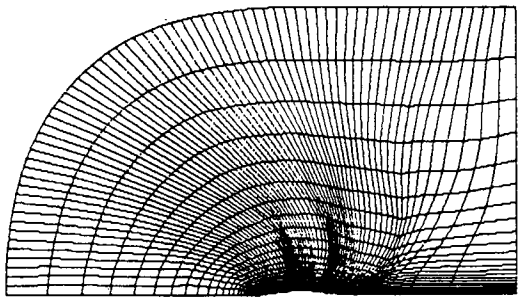

(b)

Figure 8. Surface pressure coefficient and adaptive grid at NT = 350 for $M_\infty = 1{\cdot}10$. (a) ———: computed transient C_p; ○: measured steady state C_p. (b) Adaptive grid based on variable $\bar{\lambda}_0$ and $\bar{\lambda}_v$; $\lambda = 5{\cdot}0$

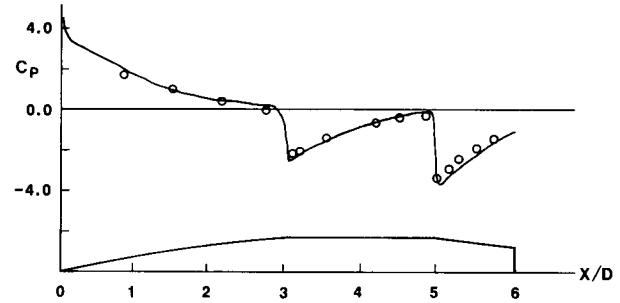

(a)

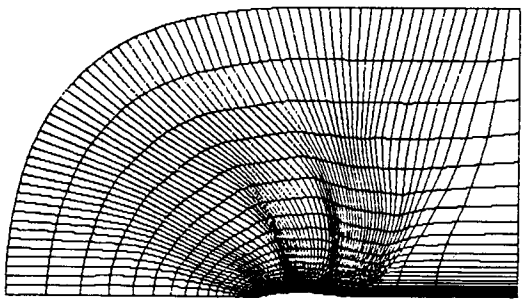

(b)

Figure 9. Converged surface pressure coefficient and adaptive grid at NT = 500 for $M_\infty = 1{\cdot}10$. (a) ——: computed transient C_p; ○: measured steady state C_p. (b) Adaptive grid based on variable $\bar{\lambda}_0$ and $\bar{\lambda}_v$; $\bar{\lambda} = 7{\cdot}5$

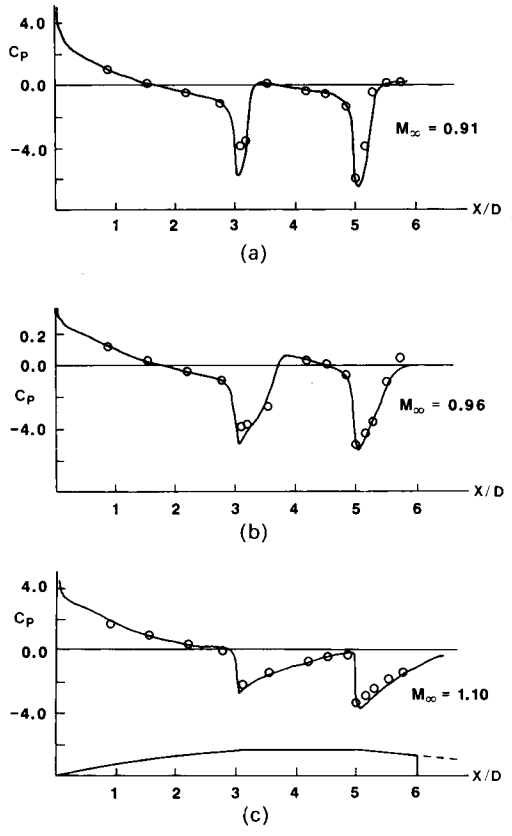

Figure 10. Converged C_p-distribution based on self-adaptive gridding; ○: measured data. (a) C_p distribution computed at NT = 650. (b) C_p distribution computed at NT = 800. (c) C_p distribution computed at NT = 500

development of the pressure field and shock waves. Exactly the same solution process has been applied without any difficulty to the projectile problem at $M_\infty = 0{\cdot}91$ and 0·96. The surface pressure coefficient computed at NT = 650 and 800 for $M_\infty = 0{\cdot}91$ and 0·96, respectively, and that of $M_\infty = 1{\cdot}10$ are shown in Figure 10 with corresponding measured data plotted for comparison.

CONCLUDING REMARKS

An adaptive grid generation technique based on variational principles has been investigated for the computation of inviscid transonic projectile aerodynamics. The isoperimetric problem for adaptive gridding is to minimize a grid smoothness functional subject to a grid orthogonality functional and a grid resolution functional. With the choice of computed pressure gradient as the control function for grid resolution, the resulting Euler equations do indeed provide a grid adaptive to the pressure field; however, for the projectile geometry considered, the normal grid resolution obtained in the boundary layer region is not sufficient, and consequently is detrimental to the convergence process of a solution algorithm for the flow problem. The difficulty is overcome by redistributing the grid points along each normal grid line by an exponential clustering technique. Moreover, for providing a better grid, the Lagrange multipliers of the isoperimetric problem have been assumed to be variables with zero variation and are chosen as functions of local grid size to enhance locally the grid resolution as well as to maintain the weight of three grid characteristics the same over the

entire flow field. Accordingly, a grid generation code has been developed and coupled to an axisymmetric thin-layer Navier–Stokes code for self-adaptive grid generation.

For the three transonic flow cases considered, the surface pressure calculated from the inviscid option of the Navier–Stokes code is indeed in excellent agreement with experimental data. The strategy of self-adaptive gridding, at an interval of 150 time steps, employed in the process of computation is an art rather than a science. For the steady transonic flow problem of interest and the use of a 70×35 planar grid, it is not necessary to generate a new grid too frequently; in fact, a strategy of self-adaptive gridding at every 100 time steps has been considered for the case $M_\infty = 0{\cdot}96$, and the accuracy of the computed surface pressure distribution is about the same as that shown in Figure 10. It is mentioned in passing that an adaptive gridding based on variational principles can be rather expensive for complex unsteady flow problems, since a new grid governed by quasilinear elliptic equations must be generated more frequently.

ACKNOWLEDGEMENT

This work was partially supported by a 1984 USAF-SCEEE research initiation programme and a 1985 USAF-UES mini-grant.

REFERENCES

1. T. H. Pulliam and J. L. Steger, 'Implicit finite-difference simulations of three-dimensional compressible flow', *AIAA Journal*, **18**, 159–167 (1980).
2. B. S. Baldwin and H. Lomax, 'Thin-layer approximation and algebraic model for separated turbulent flows', *Paper 78-257, AIAA 16th Aerospace Sciences Meeting*, January 1978.
3. C. J. Nietubicz, T. H. Pulliam and J. L. Steger, 'Numerical solution of the azimuthal-invariant thin-layer Navier–Stokes equations', *Paper 79-0010, AIAA 17th Aerospace Sciences Meeting*, January 1979.
4. J. L. Steger, C. J. Nietubicz and K. R. Heavy, 'A general curvilinear grid generation program for projectile configurations', *ARBRL-MR-03142*, U.S. Army Ballistic Research Laboratory, October 1981.
5. C. J. Nietubicz, 'Navier–Stokes computations for conventional and hollow projectile shapes at transonic velocities', *AIAA-81-1262, AIAA 14th Fluid and Plasma Dynamics Conference*, June 1981.
6. L. D. Kayser and F. Whiton, 'Surface pressure measurements on a boattailed projectile shape at transonic speeds', *ARBRL-MR-03161*, ADA 113520, U.S. Army Ballistic Research Laboratory, March 1982.
7. W. B. Sturek, 'Opportunities for application of adaptive grids in computational aerodynamics', in I. Babuska, J. Chandra and J. E. Flaherty (eds), *Proc. Adaptive Computational Methods of Partial Differential Equations*, SIAM, 1983.
8. C. W. Mastin, 'Error induced by coordinate systems', in J. F. Thompson, (ed.), *Numerical Grid Generation*, North-Holland, 1982.
9. J. U. Brackbill, 'Coordinate system control: adaptive meshes', in J. F. Thompson (ed.), *Numerical Grid Generation*, North-Holland, 1982.
10. J. Saltzman, 'A variational method for generating multidimensional grids', *Ph.D. Thesis*, New York University, 1981.
11. J. Brackbill and J. Saltzman, 'Adaptive zoning for singular problems in two dimensions', *J. Comp. Phys.*, **46**, 342 (1982).
12. R. Courant and D. Hilbert, *Methods of Mathematical Physics*, Vol. I, Interscience Publishers, 1953.